NASA Technical Memorandum 100218
ICOMP-87-6
AIAA-88-0594

Navier-Stokes Cascade Analysis With a Stiff k-ϵ Turbulence Solver

Jong-Shang Liu
Institute for Computational Mechanics in Propulsion
Lewis Research Center
Cleveland, Ohio

Peter M. Sockol
Lewis Research Center
Cleveland, Ohio

and

Joseph M. Prahl
Case Western Reserve University
Cleveland, Ohio

Prepared for the
26th Aerospace Sciences Meeting
sponsored by the American Institute of Aeronautics and Astronautics
Reno, Nevada, January 11-14, 1988

NASA

NAVIER-STOKES CASCADE ANALYSIS WITH A STIFF k-ϵ TURBULENCE SOLVER

Jong-Shang-Liu*
Institute for Computational Mechanics in Propulsion
NASA Lewis Research Center, Cleveland, Ohio

Peter M. Sockol
Computational Fluid Dynamics Branch
NASA Lewis Research Center, Cleveland, Ohio

and

Joseph M. Prahl
Department of Mechanical & Aerospace Engineering
Case Western Reserve University, Cleveland, Ohio

Abstract

The two-dimensional, compressible, thin-layer Navier-Stokes equations with the Baldwin-Lomax turbulence model and the k-ϵ model are solved numerically to simulate the flow through a cascade. The governing equations are solved for the entire flow domain, without the boundary layer assumptions. The stiffness of the k-ϵ equations is discussed. A semi-implicit, Runge-Kutta, time-marching scheme is developed to solve the k-ϵ equations. The impact of the k-ϵ solver on the explicit Runge-Kutta Navier-Stokes solver is discussed. Numerical solutions are presented for two-dimensional turbulent flow over a flat plate and a double circular arc cascade and compared with experimental data.

Introduction

In order to reduce the number of trial designs of turbomachinery, improved understanding of the physical phenomena occurring within the turbomachine is required. A wide variety of flow characteristics that exist in turbomachinery blade passages is described in detail by McNally and Sockol[1]: large pressure gradients, shock waves, shock-boundary layer interactions, and cross flows generated by vorticity field redistribution in turning flows. With the advent of large digital computers and the development of efficient numerical algorithms, numerical simulation models have become a realistic alternative to laboratory testing programs. The flow field predicted by numerical calculations can be validated with available data from experiments. If acceptable agreement is obtained, a greater level of confidence in the predictive capability of the numerical model will enhance the usefulness of the code to the designers.

The flow within turbomachinery may be laminar, transitional or turbulent, attached or separated, and wakes exist downstream of the blade rows. To obtain useful numerical predictions for such complex flows, the Navier-Stokes equations are required. Although the Navier-Stokes equations are valid for turbulent flows, the fluid variables change rapidly in space and time and can not be resolved by numerical calculations. After the compressible form of the Navier-Stokes equations are mass averaged, a turbulence model is required to obtain a closed system of equations.

The purpose of this work is to apply two turbulence models to a cascade and compare the results with available data. The two dimensional flow is studied by numerically solving the mass-averaged, compressible, thin-layer Navier-Stokes equations in conjunction with an algebraic eddy viscosity and two-equation model. The algebraic eddy viscosity model was developed by Prandtl in 1925, and modified by Cebeci et al.[2] as a two layer model. Baldwin and Lomax[3] modified it to avoid finding the edge of the boundary layer. The two-equation model, developed by Jones and Launder[4], employs less empiricism than the algebraic eddy viscosity model: the velocity and length scale are calculated. It contains two additional partial differential equations, the turbulence kinetic energy (k) and dissipation rate (ϵ) equations. The k and ϵ equations used here are in a compressible form without the boundary layer type assumptions. A two dimensional viscous code developed by Chima[5,6] using a finite-difference, explicit, two-stage, time-marching scheme is used to predict the mean flow. Since the source terms of the k and ϵ equations are stiff, a semi-implicit, Runge-Kutta, time-marching scheme is developed to calculate the k and ϵ equations.

The turbulent flow over a flat plate and the flow through a two dimensional double circular arc cascade are calculated. The comparison between the calculated and measured flow fields are presented and discussed for both the Baldwin-Lomax method (BLM) and the Jones and Launder k-ϵ method (KEM).

Formulation

Governing Equations

The equations governing the fluid motions are the compressible form of the Navier-Stokes equations. For turbulent flow, the equations are mass averaged. The system of equations is solved numerically on a body-

*Work funded under Space Act Agreement C99066-G.

conforming grid system, so the equations are transformed from the Cartesian system (x, y) to an arbitrary body-fitted coordinate system (ξ, η). The thin-layer approximation is used in the transformation. It neglects the viscous diffusion terms parallel to the body surface.

The equations are nondimensionalized by reference quantities, Chima[5], as follows,

$$\bar{t} = t/(L^*/c^*), \quad \bar{x} = x/L^*, \quad \bar{y} = y/L^*, \quad \bar{u} = u/c^*,$$
$$\bar{v} = v/c^*, \ \bar{p} = p/(\rho^* c^{*2}), \ \bar{T} = T/T_0, \ \bar{e} = e/(\rho^* c^{*2}),$$
$$\bar{H} = H/c^{*2}, \quad \bar{\rho} = \rho/\rho^*, \quad \bar{\mu} = \mu/\mu^*,$$
$$c^* = \sqrt{\frac{2\gamma R T_0}{\gamma+1}}, \quad Re = \frac{\rho^* c^* L^*}{\mu^*}, \quad Pr = \frac{\mu^* C_p}{\lambda^*}$$

The nondimensionalized, conservative form, two-dimensional, time-dependent, mass averaged, thin-layer Navier-Stokes equations are written as follows, (neglecting the overbar)

$$J\frac{\partial}{\partial t}(J^{-1}F_0) + J\frac{\partial}{\partial \xi}(J^{-1}F_1) + J\frac{\partial}{\partial \eta}(J^{-1}F_2) - \frac{1}{Re}J\frac{\partial}{\partial \eta}(J^{-1}F_4) = F_3 \tag{1}$$

$$\frac{\partial}{\partial t}(\hat{F}_0) + \frac{\partial}{\partial \xi}(\hat{F}_1) + \frac{\partial}{\partial \eta}(\hat{F}_2) - \frac{1}{Re}\frac{\partial}{\partial \eta}(\hat{F}_4) = \hat{F}_3 \tag{2}$$

$$F_0 = \begin{pmatrix} \rho \\ \rho u \\ \rho v \\ e \end{pmatrix} \quad F_1 = \begin{pmatrix} \rho U \\ \rho u U + \xi_x P \\ \rho v U + \xi_y P \\ \rho U H \end{pmatrix} \quad F_2 = \begin{pmatrix} \rho V \\ \rho u V + \eta_x P \\ \rho v V + \eta_y P \\ \rho V H \end{pmatrix}$$

$$F_3 = \begin{pmatrix} 0 \\ 0 \\ 0 \\ 0 \end{pmatrix} \quad F_4 = \begin{pmatrix} 0 \\ m_1 u_\eta + m_2 v_\eta \\ m_2 u_\eta + m_3 v_\eta \\ m_4[e/p - 1/2(u^2+v^2)]_\eta + \\ (m_1 u + m_2 v)u_\eta + (m_2 u + m_3 v)v_\eta \end{pmatrix}$$

where

$$m_1 = (4/3\eta_x^2 + \eta_y^2)(\mu + \mu_t)$$
$$m_2 = 1/3\eta_x\eta_y(\mu + \mu_t)$$
$$m_3 = (\eta_x^2 + 4/3\eta_y^2)(\mu + \mu_t)$$
$$m_4 = (\eta_x^2 + \eta_y^2)(\mu/Pr + \mu_t/Pr_t)$$

Turbulence Model

Baldwin-Lomax Model (BLM)

This model is the two layer model developed by Baldwin and Lomax[3], and has been extensively used in the literature for calculating attached and mildly separated turbulent flows.

The Prandtl-Van Driest formulation is used in the inner region to obtain μ_t. A modified Clauser formulation is used in the outer region. A simple transition criterion is formulated in this model by setting the eddy viscosity equal to zero everywhere in a profile for which the maximum tentatively computed value of μ_t is less than a specified value. The detailed formulation is omitted here and can be seen in ref. 3.

Two-Equation Model (KEM)

In this model, first introduced by Jones and Launder[4], the eddy viscosity is obtained from the turbulence kinetic energy and dissipation rate. The turbulence quantities, k and ϵ are determined from the transport equations.

The k and ϵ are nondimensionalized by k^* and ϵ^*, where $k^* = \mu^* c^*/(\rho^* L^*)$, $\epsilon^* = \mu^* c^{*2}/(\rho^* L^{*2})$. The nondimensionalized, thin-layer form of the k-ϵ equations are written in a conservative form similar to equation (1).

$$F_0 = \begin{pmatrix} \rho k \\ \rho \epsilon \end{pmatrix} \quad F_1 = \begin{pmatrix} \rho U k \\ \rho U \epsilon \end{pmatrix} \quad F_2 = \begin{pmatrix} \rho V k \\ \rho V \epsilon \end{pmatrix}$$

$$F_4 = \begin{pmatrix} (\mu + \mu_t/\sigma_k)m_5 k_\eta \\ (\mu + \mu_t/\sigma_\epsilon)m_5 \epsilon_\eta \end{pmatrix} \quad F_3 = \begin{pmatrix} S - \rho\epsilon \\ (C_1 S - C_2 \rho\epsilon)\epsilon/k \end{pmatrix} \tag{3}$$

where

$$m_5 = \eta_x^2 + \eta_y^2, \quad \mu_t = C_\mu \rho k^2/\epsilon,$$
$$n_1 = 4/3\xi_x^2 + \xi_y^2, \quad n_2 = 4/3\eta_x^2 + \eta_y^2,$$
$$n_3 = \xi_x^2 + 4/3\xi_y^2, \quad n_4 = \eta_x^2 + 4/3\eta_y^2,$$
$$n_5 = 8/3\xi_x\eta_x + 2\xi_y\eta_y, \quad n_6 = 8/3\xi_y\eta_y + 2\xi_x\eta_x,$$
$$n_7 = 2/3\xi_x\xi_y, \quad n_8 = 2/3\eta_x\eta_y,$$
$$n_9 = 2\xi_x\eta_y - 4/3\xi_y\eta_x, \quad n_{10} = 2\xi_y\eta_x - 4/3\xi_x\eta_y,$$
$$S = \mu_t(n_1 u_\xi^2 + n_2 u_\eta^2 + n_3 v_\xi^2 + n_4 v_\eta^2 + n_5 u_\xi u_\eta + n_6 v_\xi v_\eta + n_7 u_\xi v_\xi + n_8 u_\eta v_\eta + n_9 u_\eta v_\xi + n_{10} u_\xi v_\eta) - 2/3\rho k(u_\xi\xi_x + u_\eta\eta_x + v_\xi\xi_y + v_\eta\eta_y)$$

According to Launder and Spalding[8], the constants appearing in (3) are σ_k=1, σ_ϵ =1.3, C_1=1.44, C_2=1.92, C_μ =0.09, and no effort is made to change these numbers in this study.

The modeled k and ϵ equations are effective only in the fully turbulent region.[9] Treatment of the near wall region is described in the boundary condition section.

Numerical Scheme

A two dimensional viscous code developed by Chima[5,6] is used to predict the mean flow. The code employs an explicit, finite-difference, two-stage, Runge-Kutta algorithm.

$$q_1 = \hat{F}_0^{(n)} - \alpha_1 \Delta t R(\hat{F}_0^{(n)})$$
$$q_2 = \hat{F}_0^{(n)} - \Delta t R(q_1)$$
$$\hat{F}_0^{(n+1)} = q_2$$
$$\alpha_1 = 1.2 \tag{4}$$

$$R = \frac{1}{2}[(\hat{F}_{1_{i+1}}^{j} - \hat{F}_{1_{i-1}}^{j}) + (\hat{F}_{2_i}^{j+1} - \hat{F}_{2_i}^{j-1}) - \frac{1}{Re}(\hat{F}_{4_i}^{j+1} - \hat{F}_{4_i}^{j-1})]$$

The second and fourth order artificial dissipation terms are added to stabilize the scheme.

For the k and ϵ equations, it is unsuitable to use an explicit method, since the source terms of these equations are stiff. The integration of the stiff equations using an explicit method often imposes severe Δt limitations and has stability problems. A semi-implicit treatment of the source term of the k and ϵ equations is used. A two-stage, semi-implicit, Runge-Kutta scheme developed by Liu[7] is used to calculate the k and ϵ equations.

$$
\begin{aligned}
q_1 &= \Delta t[I - \Delta t a A(\hat{F}_0^{(n)})]^{-1} R(\hat{F}_0^{(n)}) \\
q_2 &= \Delta t[I - \Delta t a A(\hat{F}_0^{(n)})]^{-1} R(\hat{F}_0^{(n)} + b q_1) \qquad (5) \\
\hat{F}_0^{(n+1)} &= \hat{F}_0^{(n)} + \alpha_1 q_1 + \alpha_2 q_2
\end{aligned}
$$

$$
\begin{aligned}
R =& \frac{1}{2}[(\hat{F}_{1_{i+1}}^{j} - \hat{F}_{1_{i-1}}^{j}) + (\hat{F}_{2_i}^{j+1} - \hat{F}_{2_i}^{j-1}) \\
& - \frac{1}{Re}(\hat{F}_{4_i}^{j+1} - \hat{F}_{4_i}^{j-1})] + \hat{F}_3 \\
A =& \partial \hat{F}_3 / \partial \hat{F}_0
\end{aligned}
$$

The coefficients a, b, α_1, and α_2 are obtained by matching (5) with the Taylor series expansion of $\hat{F}_0^{(n+1)}$ to second order in time and by letting the characteristic root go to zero as t goes to infinity.

$$a = b = \alpha_1 = 1.7071, \quad \alpha_2 = -1.7071$$

The convection terms are evaluated explicitly and the source term semi-implicitly. The two by two Jacobian matrix from the source term is evaluated once for every two stage calculation. A local time step is used to accelerate convergence to a steady state.

The impact of the k-ϵ equation on the main code is introduced in the following way.

(i) The main flow field is calculated with the BLM method for 1000 time steps.
(ii) The flow field variables are fixed and the k and ϵ equations are calculated for 1000 time steps.
(iii) The k and ϵ values are fixed and the mean flow field is calculated for 10 time steps.
(iv) The flow field is fixed and k and ϵ are calculated for 10 time steps.
(v) Step (iii) and (iv) are repeated until convergence to steady state is achieved.

Stability Analysis

The numerical stability is analyzed in the inviscid parts of the governing equations. By linearizing the inviscid parts of the conservative form of the equations and applying the Von Neumann stability criterion, the stability limitation on the time step for the mean flow and k-ϵ equation can be found. The Δt limitation for the mean flow is

$$\Delta t < 1/[U + V + c\sqrt{(\xi_x + \eta_x)^2 + (\xi_y + \eta_y)^2}\,].$$

The Δt limitation for the k-ϵ equation can not be shown in explicit form, see ref. 7 for the detail.

Boundary Conditions

For subsonic inflow, the three incoming characteristic speeds are replaced by three boundary conditions: total pressure, total temperature, and flow angle. Small values of k and ϵ are specified at the inlet. The upstream-running Riemann invariant is extrapolated from the interior. For subsonic outflow, the static pressure is specified at the downstream boundary and other properties are extraploated from the interior. No-slip conditions and the wall temperature are specified on the wall. The pressure on the wall is calculated through the normal momentum equation.

Since the k and ϵ equations are only effective in a fully turbulent region, they are not applied directly to the wall. Many modifications are required to calculate k and ϵ near the wall. A review of the low Reynolds number two-equation model given by Patel, Rodi and Scheuerer[9] bases the modifications largely on numerical experiments and comparisons with different flows, and it is not clear which models can be used with confidence. Near the wall, the values of k and ϵ change very rapidly, and many grid points are needed to predict k and ϵ there. In this study, the BLM method is used to predict μ_t, and from the assumption of local equilibrium, values of k and ϵ near the wall are found, ($y^+ < 40$). This method does not need to modify the equations, is easy to calculate, and does not appear to require very fine grids near the wall.

Results and Discussion

Numerical results are presented for turbulent flow over a flat plate and for flow over a two-dimensional double circular arc cascade.

Flat Plate Problem

The subsonic flow over a zero thickness flat plate cascade with zero stagger angle is calculated comparing the KEM and BLM turbulence models. The flat plate of chord C and zero thickness has a pitch of 0.2C. Because of symmetry, the computational domain is one half of the flow passage. The inlet boundary is 0.1C upstream of the leading edge of the plate. The flow with an inlet Mach number of 0.5 and zero angle of attack is calculated for this case. The minimum grid space Δx is 0.0025C in the near leading edge region and smoothly stretched up and downstream. The minimum grid space Δy is 10^{-6}C and the grid is smoothly stretched away from the wall.

In Fig. 1 the computed local skin friction coefficient versus Reynolds number based on the distance from the leading edge is compared with the Karman-Schoenherr skin friction correlation[10], Wieghardt[11] data and the correlation from Schlichting[12]. The numerical results of the two models compare well with the data, with the BLM predicting a higher C_f than that predicted by KEM

for Re_x greater than 10^6. The predicted behavior in the range $10^5 < Re_x < 10^6$ is due either to the effect of the singular point at the leading edge or to the flow not being fully turbulent in that region. Figs. 2 and 3 show the velocity distribution. In Fig. 2, the mean velocity, nondimensionalized by the free stream velocity, is plotted versus the distance from the wall, nondimensionalized by the displacement thickness. KEM and BLM predict the same results in excellent agreement with the data of Klebanoff and Diehl[13]. In the near wall region, u^+ is shown versus y^+ in Fig. 3. The numerical results agree in the sublayer region. In the log-wall region, the predicted Karman constant is about 0.4, however the predicted u^+ is smaller than data of Schlichting[12], Klebanoff[13] and Hinze[14]. This is most likely due to a lack of enough grid points in the region $10 < y^+ < 50$.

The distribution of the turbulent shear stress at Re_δ = 80000 is compared with the data of Klebanoff[15] in Fig. 4 and that of Schubauer[16] in the near wall region in Fig. 5. Near the wall, the computed turbulent shear stress is nearly constant and agrees favorably with the data. The discrepancies increase as y/δ increases. This is probably attributable to grid size effect. The BLM predicts slightly higher turbulent shear stresses than that predicted by KEM. The KEM and BLM results are virtually identical in the near wall region and agree within experimental error with the data (Fig. 5).

The turbulent kinetic energy and dissipation rate profile from the KEM calculations are shown in Figs. 6 to 8. The computed k distribution is compared to the data of Klebanoff[15] in Fig. 6. The computed k agrees well with the data except near the wall. The k distribution in inner variables is compared to the results of Patel et al.[9] in Fig. 7. k^+ is underpredicted in the inner region and no peak of k^+ is predicted because the KEM is only effective in the fully turbulent region. In the sublayer and buffer region ($y^+ < 40$), the assumption that turbulence production is equal to dissipation rate is used. The dissipation rate is over-predicted in these regions (Fig. 8). Some modified versions of the two-equation model can predict the existance of the peak of k^+.[9] However, most of the modifications are based on numerical experiments, without physical basis and applied to specific flows. Since the basic two-equation model can predict the mean flow well except very near the wall, the local equlibrium assumption and the zero-equation model are used in the near-wall region where KEM is ineffective or requires further questionable modifications.

Double Circular Arc Cascade

Numerical calculations for flow over a two dimensional double circular arc cascade are compared with data obtained on a blade section designed by Sanger at NASA Lewis Research Center and tested at Pennsylvania State University by Deutsch and Zierke[17,18].

The blade section is a double circular arc with a camber of 65 degrees and a chord length of 228.6 mm, machined round to a 9.14 μm radius at the leading and trailing edges. The equations for the blade surface geometry, and camber line are given in [17]. In the Penn. state experiment, a five blade cascade was tested. The solidity (chord length/pitch length) of the cascade was 2.14 and the stagger angle was 20.5 degrees in the test. The measurements were made in air at a chord Reynolds number based on inlet conditions of 500,000 and a positive incidence angle of 5 degrees. The inlet velocity, 33.11 m/sec (about Mach 0.1), was measured by a five-hole probe approximately 38 mm upstream of the blade leading edge. A one-component laser Doppler velocimeter (LDV) was used to measure the flow field in the experiment, and the five-hole probe was used to make inlet and outlet measurements. The two dimensionality in the experiment was controlled by adjusting the lower and upper false blade positions, the tailboard position, and the magnitude of top, side and upper-channel suction. The periodicity of the cascade was controlled by side wall suction.[17]

The computational domain covers one blade passage of the cascade. The upstream boundary is located about sixty percent chord upstream of the leading edge and the downstream boundary is located about sixty percent chord downstream of the trailing edge. The interior body-fitted grids of this domain are generated using the GRAPE code developed by Sorenson[19]. This grid generation code generates a two dimensional grid about arbitrary boundaries by iteratively solving two coupled Poisson equations. Two C-type grids with (257 x 65) and (129 x 33) points are used in the numerical calculations.

Fig. 9 shows a comparison of the calculated and measured blade static pressure distributions. The pressure surface has a large favorable pressure gradient near the leading edge. As the flow proceeds, the pressure gradient is mildly adverse and becomes favorable again further downstream. The suction surface has a large unfavorable pressure gradient near the leading edge and a flat pressure profile near the trailing edge as seen from the data. The pressure distribution on the pressure surface predicted by the coarse grid calculation is identical with the fine grid calculation. The predicted pressure distribution on the suction surface by the fine and coarse grids are different before 40 percent cord and after 70 percent chord because the resolution of the coarse grid is not fine enough to pick up the rapidly changing flow properties on the suction surface. The results predicted by a laminar flow calculation also shown in Fig. 9 do not predict the turbulent flow well, especially on the suction surface. The KEM and BLM results show similar results for pressure distribution. Both predictions are in good agreement with data over the forward portion of the blade. The real flow tends to separate and becomes unsteady after sixty percent chord on the suction surface, and the discrepancies increase especially on the suction surface. The KEM predicts slightly better agreement with data than BLM on the aft portion of the blade.

Calculated pressure and Mach contour are given in Fig. 10 and 11. No measured contours are available. Large pressure gradients occur near the leading edge on

both the pressure and suction surface. Small pressure gradients exist on the pressure surface aft of the leading edge while still large pressure gradients persist on the suction surface. In the wake, there are small pressure gradients indicated on the pressure contours. The stagnation point is on the pressure surface because of the high incidence angle. The high velocity generated near the leading edge of the suction surface is a result of flow acceleration from the stagnation point around the blade leading edge. When the flow proceeds further on the suction surface, and is subjected to a large adverse pressure gradient, the flow becomes unstable and transition to turbulence happens rapidly.[17] The growth of the boundary layer on the suction surface and the wake development downstream of the trailing edge are evident in the Mach number contours (Fig. 11).

The velocity distributions were measured at eleven chordwise locations on both the pressure and suction surfaces, and the data have ninty-five percent confidence bands. (except near the leading edge thin boundary layer and near the trailing edge unsteady flow).[17] Since the computational grids are non-orthogonal and not coincident with the measurement locations, two-dimensional linear interpolation[20] is used to obtain the computed velocities at the measurement locations to compare with data. Comparisons of the calculated and measured velocity distributions at six chordwise locations on the suction surface are shown in Fig. 12. y is the normal distance from the wall and u is the velocity component parallel to the wall. The flow over all of the suction surface is turbulent because the large adverse pressure gradient near the leading edge triggers early transition. The calculations agree with the data well near the leading edge, with the BLM showing marginally better agreement with the data than the KEM. Both models predict less flat velocity profiles than the data, possibly because of deficiencies in the turbulence models which can not handle high curvature and pressure gradient effects well or because insufficient resolution of the boundary layer in the numerical calculations underpredicts the turbulence near the wall. The KEM results have better agreement than BLM after 50 percent chord. After 60 percent chord on the suction surface, the flow tends to separate and become unsteady. The KEM predicts separation after 90 percent chord and no separation is predicted by the BLM calculation.

Fig. 13 compares the calculated and measured velocity distributions at six chordwise locations on the pressure surface. At the leading edge on the pressure surface, because of the large incidence angle, the favorable pressure gradient maintains a laminar flow. The data shows a mildly adverse pressure gradient following the leading edge high favorable pressure gradient. Further downstream, the pressure gradient again becomes favorable and a fully turbulent flow does not develop on the pressure surface. The results from both the KEM and BLM calculations are similar on the pressure surface. The flow on the pressure surface is well behaved with no separation since there are no strong adverse pressure gradients to trigger separation, transition, or reattachment.

Measurements of the wake were made at three locations, two near wake and one far wake locations. The near wake data were taken at 105.4 and 109.6 percent chord positions. The percent chord given here is actually the percent of total pressure surface blade arc. The origin of y is along the extended arc from the pressure surface and y is positive on the pressure side of the curve. The far wake data were taken at 152.6 percent chord position. The origin of y is located along the tangent curve of the camber line at the trailing edge. The LDV technique was used to measure the flow field in the near wake and the five-hole probes were used to measure the flow in the far wake. Fig. 14 shows the velocity distribution in the near wake. The flow in the near wake is asymmetric because the suction surface and pressure surface boundary layers that merge at the trailing edge are different in shape and thickness. The KEM results are closer to the data than the BLM results, but there remains substantial disagreement between prediction and measurements. The velocity distribution data and predictions in the far wake shown in Fig. 15 are approaching symmetric profiles. The center line of the wake is moved to the suction side because of the smaller velocity near the trailing edge on the suction surface than on the pressure surface, and because of the pressure difference between these two surfaces. The computed center line of the far wake is closer to the pressure side than that measured because the computed trailing edge velocity on the suction surface is higher than that measured.

Conclusion

A numerical solution of the two dimensonal, compressible, turbulent cascade flow field problem comparing the Baldwin-Lomax (BLM) and the k-ϵ (KEM) turbulence models is solved using a two-stage, explicit, Runge-Kutta, time-marching code for the mean flow. The stiffness of the k and ϵ equations necessitates a semi-implicit, Runge-Kutta, time marching scheme to solve the thin-layer type k-ϵ equations. No special effort is made in modifying the model constants to improve agreement between predictions and measurements in this study. The local equilibrium assumption and the BLM is used to predict the values of k and ϵ near the wall in the KEM calculation. No wall function or low Reynolds number k-ϵ modification is used. Numerical solutions are obtained for two dimensional, compressible, turbulent flow over a flat plate and a double circular arc cascade and compared with data.

Flow over a flat plate with an inlet Mach number of 0.5 is calculated comparing the KEM and BLM turbulence models. Both the KEM and BLM results are similar and compare favorably with experimental data. For this simple geometry with no pressure gradients, flow separation or surface curvature, the BLM is sufficient to predict the mean flow field. The use of a higher-order turbulence model does not have advantage over the BLM.

For the double circular arc cascade flow at an inlet Mach number of 0.1, both the KEM and BLM predict nearly identical surface pressure distributions. The KEM

predicts velocity profiles that agree better with data than those predicted by BLM near the trailing edge separation region on the suction surface. Although the KEM results are closer to the data than the BLM results, there remains substantial disagreement between prediction and measurements. The discrepancies between the computations and the experimental data arise from both inadequacies in the turbulence model and numerical effects. The grid resolution in the surface normal direction and in the streamwise direction have an influence on the numerical accuracy. An adapative grid may be needed in the calculation where the flow properties change rapidly. The thin-layer approximation in the calculation might be unsuitable since the flow properties change rapidly along the streamline, especially near the leading and trailing edges.

For flow over complex geometries with pressure gradients or separation, the BLM is not adequate and a higher-order turbulence model is needed. The application of KEM to complex flow geometries needs improvements to handle the low-Reynolds number flow near the wall, flow transition, and separation. It also requires improvements in computational efficiency to make the KEM calculation competitive with the BLM calculation.

References

1. McNally, W. D. and Sockol, P. M., "Computational Method for Internal Flows with Emphasis on Turbomachinery," NASA TM 82764, 1981.
2. Cebeci, T., Smith, A. M. O. and Mosinskis, G., "Calculation of Compressible Adiabatic Turbulent boundary Layers," AIAA Journal, Vol 8, Nov. 1970, pp. 1974-1982.
3. Baldwin, B. S. and Lomax, H., "Thin Layer Approximation and Algebraic Model for Separated Turbulent Flows," AIAA paper 78-257, 1978.
4. Jones, W. P. and Launder, B. E., "The Prediction of Laminarization with a Two-Equation Model of Turbulence," International Journal of Heat and Mass Transfer, Vol 15, 1972, pp. 301-314.
5. Chima, R. V. and Johnson, G. M., "Efficient Solution of Vectorized Multiple-Grid Algorithm," NASA TM 83376, 1983.
6. Chima, R. V., "Analysis of Inviscid and Viscous Flows in Cascades with an Explicit Multiple-Grid Algorithm," NASA TM 83636, 1984.
7. Liu, J. S., "Navier-Stokes Cascade Analysis with the k-ϵ Turbulence Model", Ph. D. Dissertation, Case Western Reserve University, May 1987.
8. Launder, B. E. and Spalding, D. B., "The Numerical Computation of Turbulent Flows," Computer Methods in Applied Mechanics and Engineering, Vol 3, 1974, pp. 269-289.
9. Patel, V. C., Rodi, W. and Scheuerer, G., "Turbulence Models for Near-Wall and Low Reynolds Number Flows: A Review," AIAA Journal, Vol 23, Sep. 1984, pp. 1308-1319.
10. von Karman, T., "Turbulence and Skin Friction," Journal of the Aeronautical Sciences, Vol. 1, Jan. 1934, pp. 1-20.
11. Wieghardt, K., in AFOSR-IFP-Stanford Conference on Computation of Turbulent Boundary Layers-1968, Vol. II, Ed. by Coles, D. E. and Hirst, E. A., 1968.
12. Schlichting, H., Boundary Layer Theory, McGraw-Hill Book Co., New York, 1960.
13. Klebanoff, P. S. and Diehl, Z. W., "Some Features of Artifically Thickned Fully Developed Turbulent Boundary Layers with Zero Pressure Gradient," NACA TN 2475, 1951.
14. Hinze, J. O., Turbulence, McGraw-Hill Book Co., New York, 1975.
15. Klebanoff, P. S., "Characteristics of Turbulence in a Boundary Layer with Zero Pressure Gradient," NACA Rep. 1247, 1955
16. Schubauer, G. B., "Turbulent Processes as Observed in Boundary Layer and Pipe," Journal of Applied Physics, Vol 25, Feb. 1954, pp. 188-196.
17. Deutsch, S. and Zierke, W. C., "The Measurement of Boundary Layers on a Compressor Blade in Cascade at High Positive Incidence Angle, Part I Experimental Techniques and Results," NASA CR 179491, Aug. 1986.
18. Deutsch, S. and Zierke, W. C., "The Measurement of Boundary Layers on a Compressor Blade in Cascade at High Positive Incidence Angle, Part II Data Report," NASA CR 179492, Aug. 1986.
19. Sorenson, R. L., "A Computer Program to Generate Two-Dimensional Grids About Airfoils and Other Shapes by the Use of Poisson's Equation," NASA TM 81198, May 1980.
20. Katsanis, T. and McNally, W. D., "Revised Fortran Program for Calculating Velocities and Streamlines on the Hub-Shroud Midchannel Stream Surface on an Axial, Radial or Mixed-Flow Turbomachine or Annular Duct, Part II Programmer's Manuual," NASA TN D-8431.

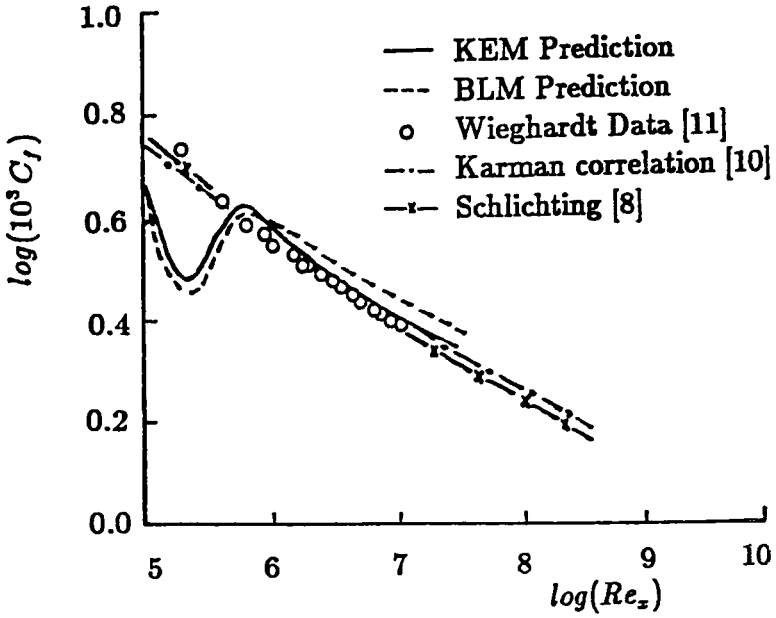

Fig. 1 Comparisons of the computed and measured local skin friction coefficient over a flat plate

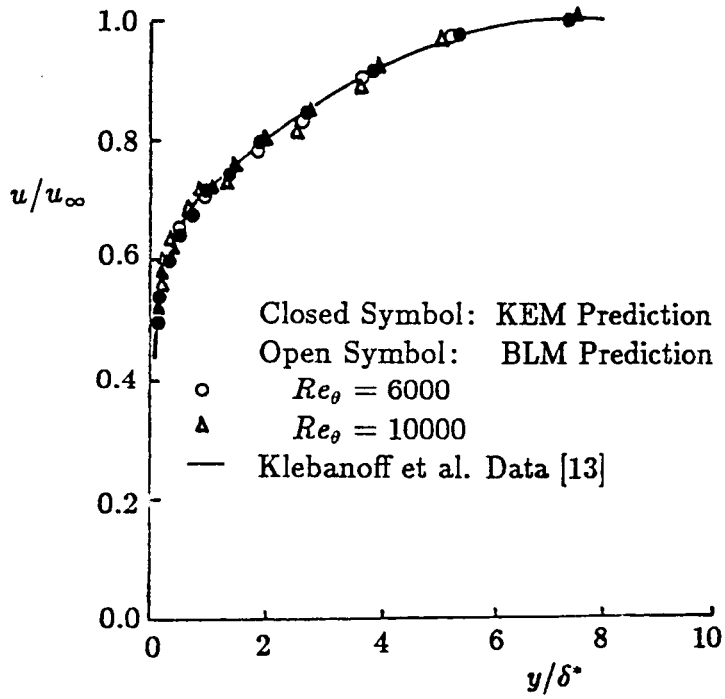

Fig. 2 Comparisons of the computed and measured velocity distribution

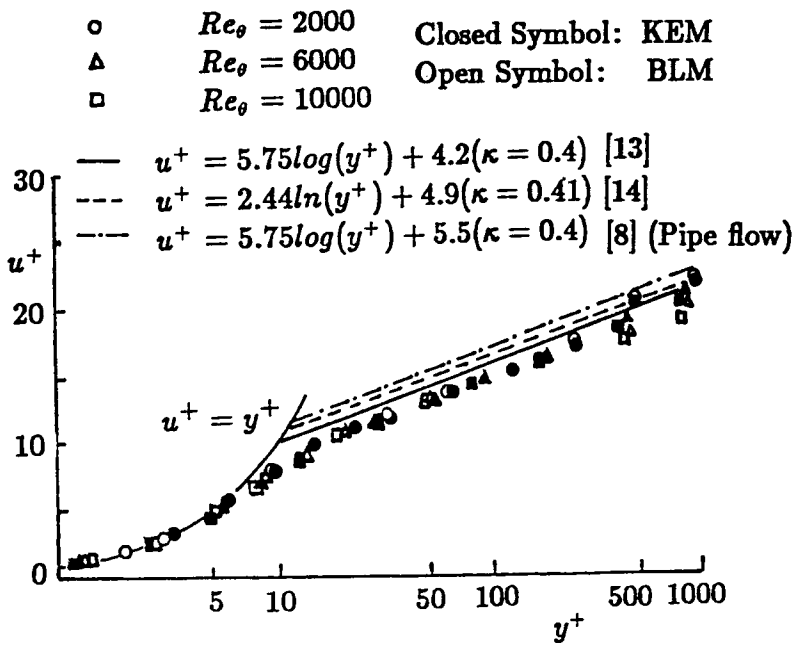

Fig. 3 Comparisons of the computed and measured velocity distribution in inner variables

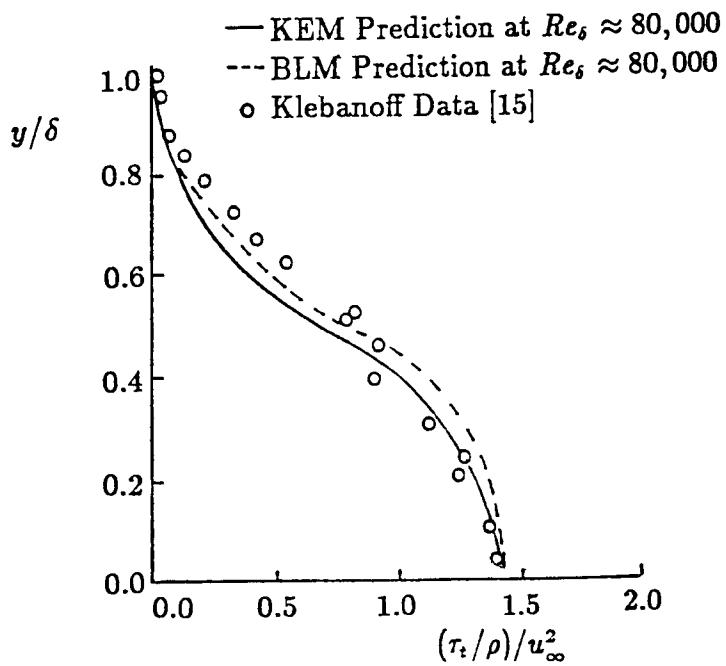

Fig. 4 Comparisons of the computed and measured turbulent shear stress distribution

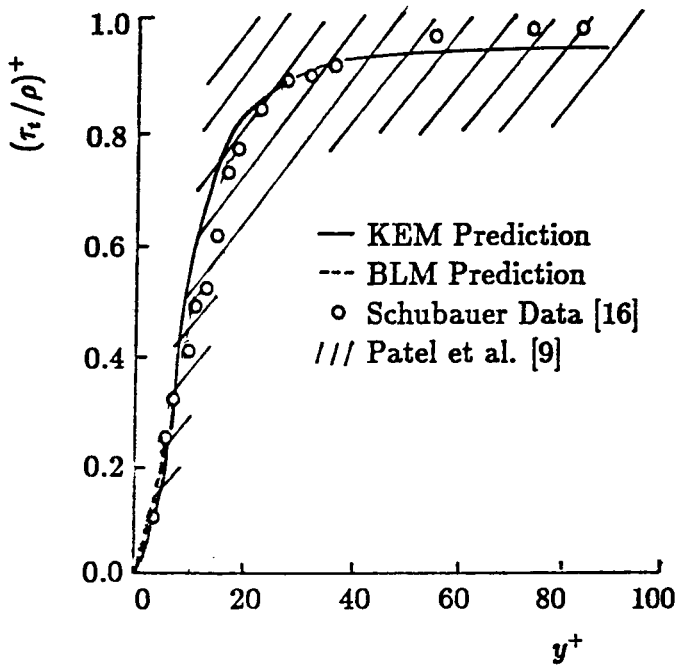

Fig. 5 Comparisons of the computed and measured turbulent shear stress distribution in inner variables

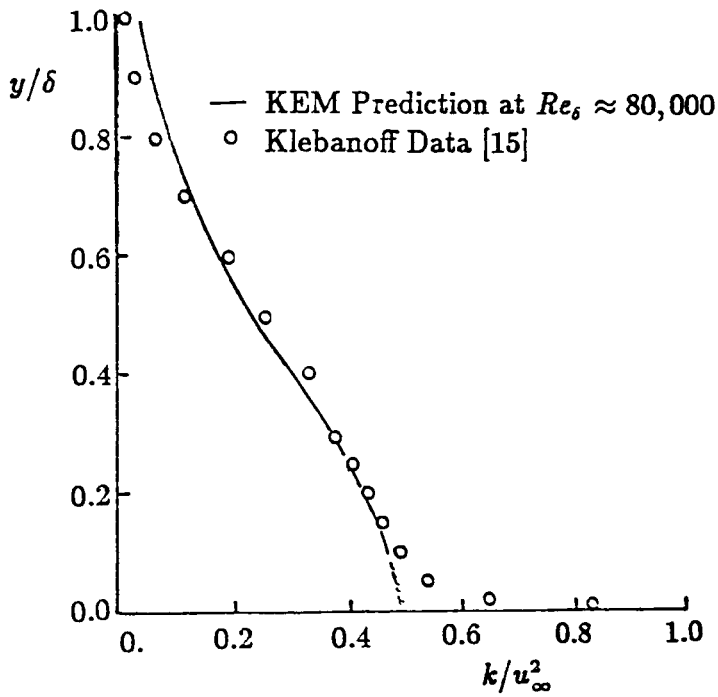

Fig. 6 The turbulent kinetic energy distribution

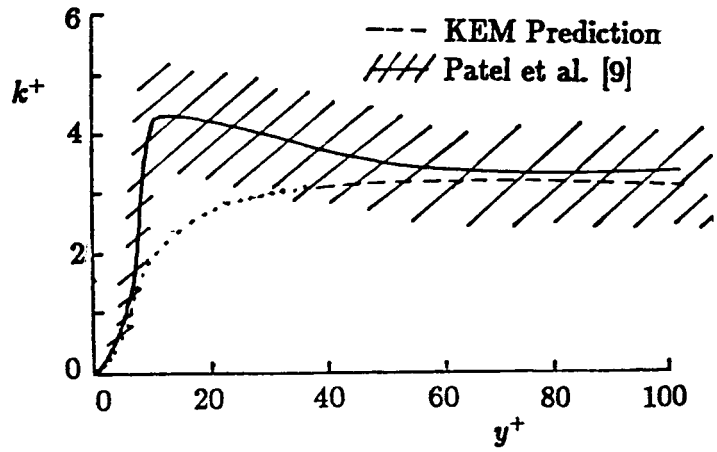

Fig. 7 The turbulent kinetic energy distribution in inner variables

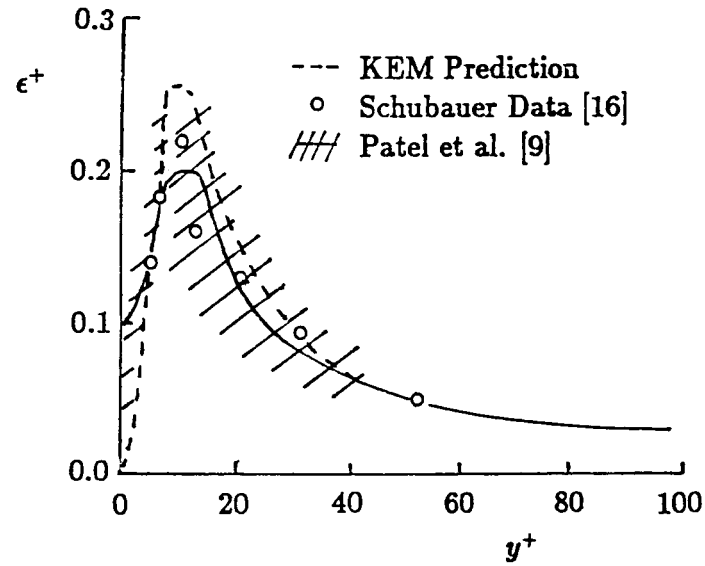

Fig. 8 The dissipation rate distribution in inner variables

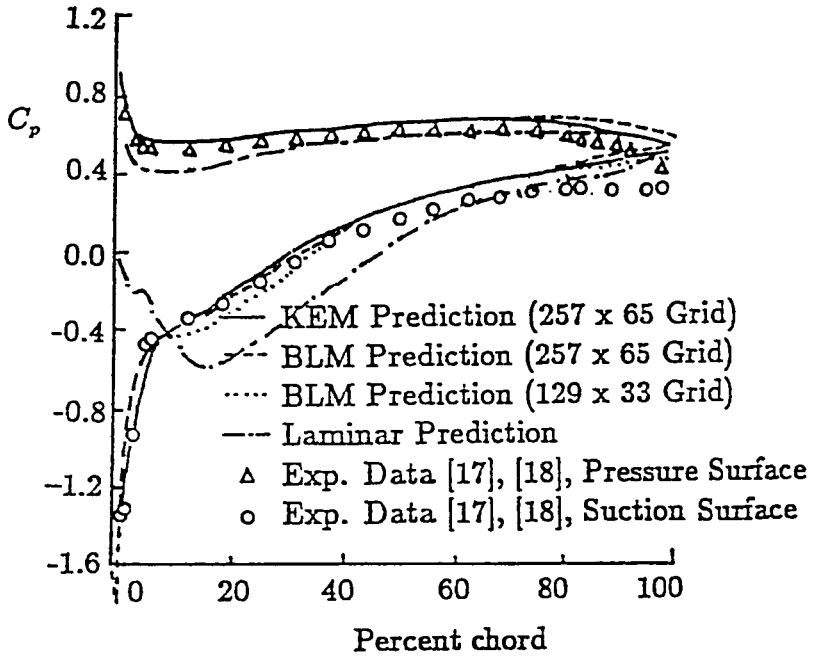

Fig. 9 Comparisons of the computed and measured blade static pressure distribution

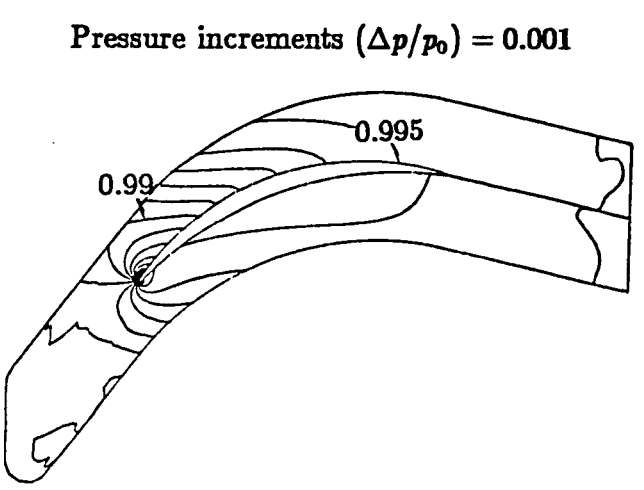

Fig. 10 Calculated pressure contours

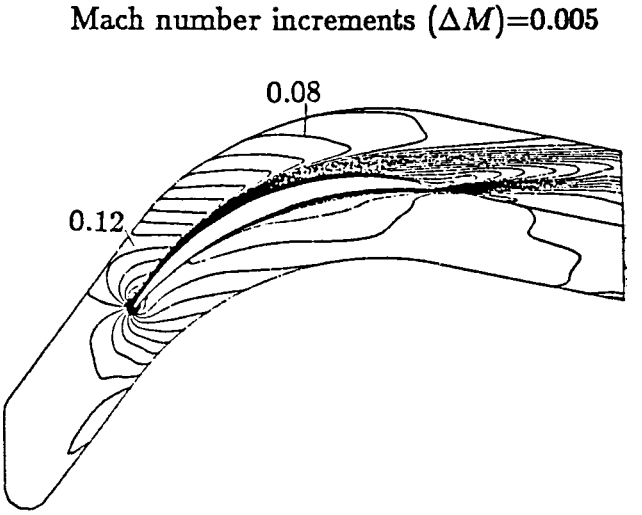

Fig. 11 Calculated Mach number contours

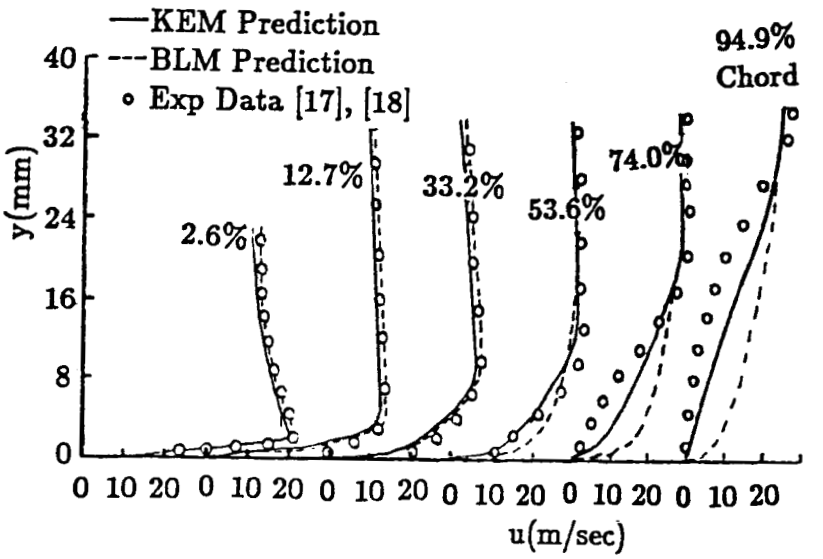

Fig. 12 Comparisons of the computed and measured velocity distribution on the suction surface

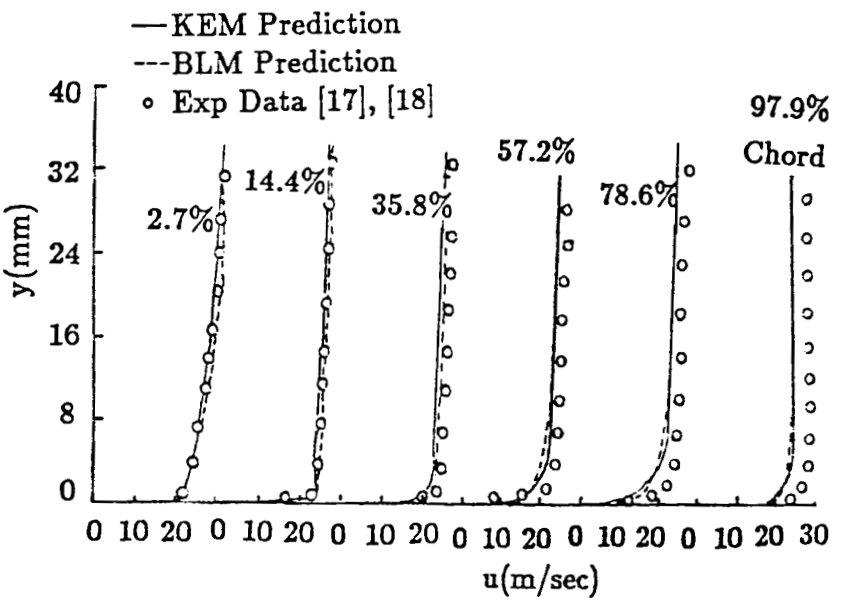

Fig. 13 Comparisons of the computed and measured velocity distribution on the pressure surface

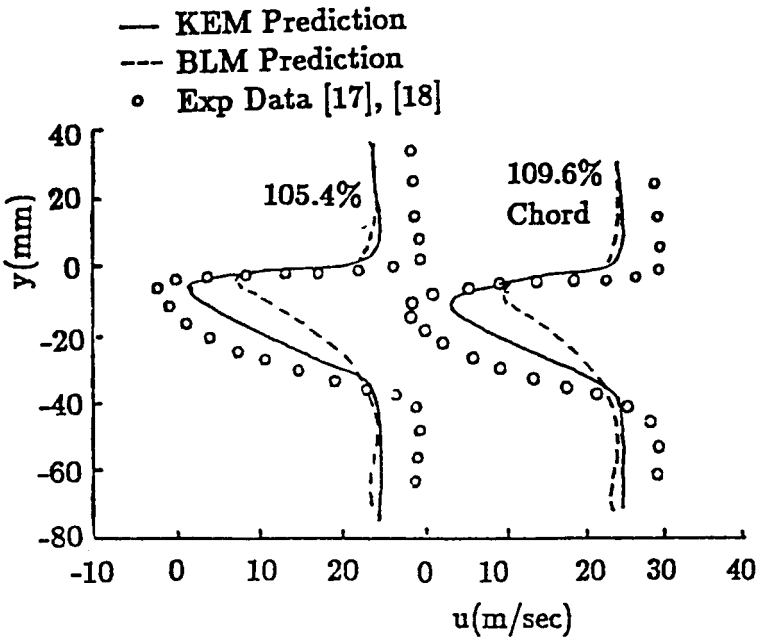

Fig. 14 Comparisons of the computed and measured velocity distribution in the near wake

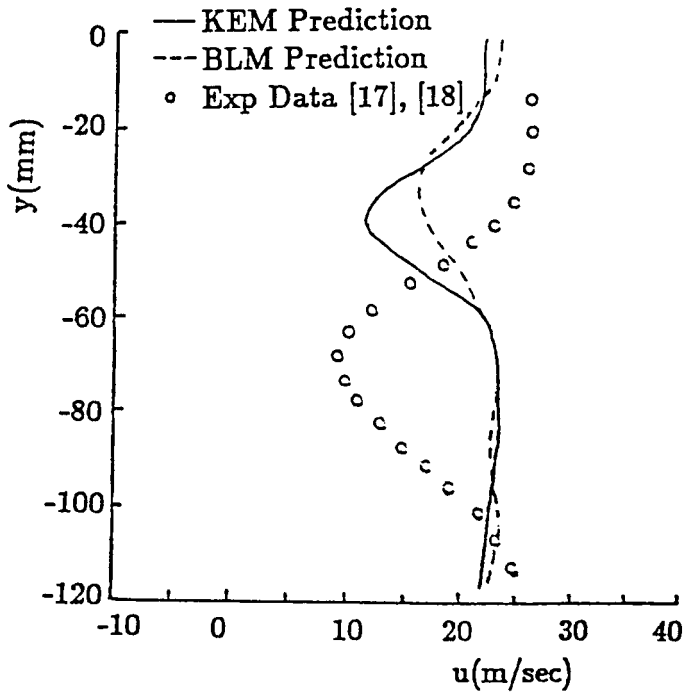

Fig. 15 Comparisons of the computed and measured velocity distribution in the far wake

NASA
National Aeronautics and Space Administration

Report Documentation Page

1. Report No.	2. Government Accession No.	3. Recipient's Catalog No.
NASA TM-100218 ICOMP-87-6; AIAA-88-0594		

4. Title and Subtitle

Navier-Stokes Cascade Analysis With a Stiff k-ϵ Turbulence Solver

5. Report Date

6. Performing Organization Code

7. Author(s)

Jong-Shang Liu, Peter M. Sockol, and Joseph M. Prahl

8. Performing Organization Report No.

E-3829

10. Work Unit No.

505-62-21

9. Performing Organization Name and Address

National Aeronautics and Space Administration
Lewis Research Center
Cleveland, Ohio 44135-3191

11. Contract or Grant No.

13. Type of Report and Period Covered

Technical Memorandum

12. Sponsoring Agency Name and Address

National Aeronautics and Space Administration
Washington, D.C. 20546-0001

14. Sponsoring Agency Code

15. Supplementary Notes

Prepared for the 26th Aerospace Sciences Meeting, sponsored by the American Institute of Aeronautics and Astronautics, Reno, Nevado, January 11-14, 1988. Jong-Shang S. Liu, Institute for Computational Mechanics in Propulsion, NASA Lewis Research Center (work funded under Space Act Agreement C99066G). Peter M. Sockol, NASA Lewis Research Center. Joseph M. Prahl, Department of Mechanical and Aerospace Engineering, Case Western Reserve University, Cleveland, Ohio 44106.

16. Abstract

The two-diminensional, compressible, thin-layer Navier-Stokes equations with the Baldwin-Lomax turbulence model and the k-ϵ model are solved numerically to simulate the flow through a cascade. The governing equations are solved for the entire flow domain, without the boundary layer assumptions. The stiffness of the k-ϵ equations is discussed. A semi-implicit, Runge-Kutta, time-marching scheme is developed to solve the k-ϵ equations. The impact of the k-ϵ solver on the explicit Runge-Kutta Navier-Stokes solver is discussed. Numerical solutions are presented for two-dimensional turbulent flow over a flat plate and a double circular arc cascade and compared with experimental data.

17. Key Words (Suggested by Author(s))	18. Distribution Statement
Turbomachinery cascades Navier-Stokes equations Turbulence model	Unclassified – Unlimited Subject Category 02

19. Security Classif. (of this report)	20. Security Classif. (of this page)	21. No of pages	22. Price*
Unclassified	Unclassified	14	A02

*For sale by the National Technical Information Service, Springfield, Virginia 22161